Journal of Modern Optics
Vol. 57, No. 19, 10 November 2010, 1900–1907

Taylor & Francis
Taylor & Francis Group

Quantum fluid properties of polaritons in semiconductor microcavities

A. Amo[a], S. Pigeon[b], C. Adrados[a], J. Lefrère[a], C. Ciuti[b], I. Carusotto[c], R. Houdré[d], A. Bramati[a] and E. Giacobino[a]*

[a]*Laboratoire Kastler Brossel, Université Pierre et Marie Curie, Ecole Normale Supérieure et CNRS, UPMC Case 74, 4 place Jussieu, 75252 Paris Cedex 05, France;* [b]*Laboratoire Matériaux et Phénomènes Quantiques, Université Paris Diderot, 75013 Paris, France;* [c]*INO-CNR BEC Center and Dipartimento di Fisica, Universita di Trento, I-38123 Povo, Italy;* [d]*Institut de Physique de la Matière Condensée, Ecole Polytechnique Fédérale de Lausanne (EPFL), Station 3, CH-1015 Lausanne, Switzerland*

(*Received 24 March 2010; final version received 7 September 2010*)

In semiconductor quantum wells embedded in a high finesse microcavity, excitons, which are bound electron-hole systems, strongly couple to photons, forming mixed quasi-particles called polaritons. Polaritons can be coherently excited by an incident laser field and detected through the emitted light. Thanks to their excitonic component, polaritons have binary interactions which can modify their dispersion curve. These properties have allowed us to demonstrate nonlinear and quantum optical effects in the microcavity emission, and more recently quantum fluid properties. A semiconductor microcavity polariton fluid, injected by a nearly-resonant continuous wave pump laser can exhibit collective excitations that deeply modify its propagation. Superfluid behavior of the polariton fluid is obtained and manifests itself as the suppression of scattering from defects. In other conditions Cerenkov-like patterns are observed. Microcavity polaritons are thus very good tools for exploring the physics of non-equilibrium quantum fluids.

Keywords: quantum fluids; exciton polariton; semiconductor microcavity

1. Introduction

For more than 10 years, semiconductor microcavities have raised a growing interest, both for their optoelectronic properties and for their quantum fluid properties [1]. Semiconductor microcavities are made of one or several very thin layers of a semiconductor material, called quantum wells, embedded in a semiconductor substrate with a different bandgap. On each side of the substrate, high quality Bragg mirrors are deposited, forming a Fabry–Perot cavity. The thickness of the cavity is of the order of one or a few wavelengths. In bulk semiconductors, optical excitation can generate excitons, light-mass Bose particles consisting of bound electron hole pairs. In a quantum well with a thickness of the order of a few nanometers, the kinetic energy of the excitons is quantized in the direction perpendicular to the well, whereas it is free within the plane of the well. In high finesse semiconductor microcavities, the large excitonic oscillator strength allows the strong coupling regime to be reached [2]. As a result, the degeneracy at resonance between the exciton mode and the photon mode is lifted and the so-called vacuum Rabi splitting takes place. The coherent exchange of energy between excitons and photons can be described in terms of half-matter half-light bosonic quasiparticles named polaritons [3].

These composite bosons have very interesting properties. Due to their photon component, polaritons with a given transverse wave vector k can be directly created by an incident laser beam with the appropriate energy and momentum. For the same reason, the angular distribution of the emission provides information about the polariton population along the dispersion curve [4]. The exciton part is responsible for the coupling between polariton modes via the Coulomb and exchange interaction, which is at the origin of optical nonlinear effects. The system has many similarities with an optical parametric oscillator (OPO) [5,6]. These nonlinearities have allowed to demonstrate parametric amplification [7,8] and later, optical bistability [9], quantum squeezing [10], generation of bright correlated beams [11,12].

On the other hand, exciton-polaritons in semiconductor microcavities have for quite some time appeared as good candidates for Bose–Einstein condensation and quantum fluid properties, essentially

*Corresponding author. Email: elg@spectro.jussieu.fr

ISSN 0950–0340 print/ISSN 1362–3044 online

DOI: 10.1080/09500340.2010.522739
http://www.informaworld.com

due to their very small effective mass, providing a large critical temperature for condensation [13–15]. The dispersion of the cavity polariton modes around $k=0$ (where k is the wave vector in the plane of the microcavity), due to the optical confinement along the z direction, results in a typical polariton effective mass of the order of 5×10^{-5} times the free electron mass. Bose–Einstein condensation under non-resonant pumping has been reported by several groups [16,17]. In spite of the short polariton lifetime, of the order of a few picoseconds, polariton-polariton scattering processes are fast enough under high excitation to produce a thermalized polariton gas, even if full thermalization cannot be achieved with the host lattice. Along the same lines, vortices [18] and persistent currents [19] have been observed in these fluids.

When the lower polariton branch is pumped by a resonant laser beam, no spontaneous quantum coherence can be demonstrated, because of the coherence injected by the laser. However, at high enough densities, the exciton polariton system has been predicted to be a quantum fluid, which exhibits collective excitations [20,21]. In this paper, we present a study of the properties of a polariton quantum fluid injected into a planar microcavity by a resonant laser. In the presence of static defects, the response of the system is modeled using a linearized theory analogous to the Bogoliubov theory of the weakly interacting Bose gas. We demonstrate superfluidity using the Landau criterion. When the polariton density reaches a critical value, the polariton fluid flows without friction and the usual scattering on defects disappears. This occurs when the flow velocity imprinted by the exciting laser is slower than the sound velocity in the polariton fluid [22]. In the supersonic regime, superfluid propagation is replaced by the appearance of a Cerenkov-like perturbation produced by the defect. A similar phenomenology was observed in [23] under a different pumping scheme, using an OPO configuration. These new effects are quite similar to the ones observed in ultra-cold atomic ensembles.

2. Quantum fluid model

In our experiments, in order to probe superfluidity we study the perturbation that is produced in an optically created moving polariton fluid when a microcavity static defect is present in the flow path, as proposed in [20,21]. This procedure is a direct application to the polariton system of the standard Landau criterion of superfluidity [24] originally developed for liquid Helium and recently applied to demonstrate superfluidity of atomic BECs [25,26]. First we present a simple model for the polariton system, with a Hamiltonian including the linear exciton photon interaction and the exciton-exciton interaction [5]. We then write the Gross Pitaevskii equation, which allows us to predict the behavior of the polariton fluid in various conditions [20].

Under low excitation, the linear Hamiltonian for excitons and photons in the cavity is $H=\sum_{\mathbf{k}}H_{\mathbf{k}}$ with

$$H_{\mathbf{k}}=E_X(k)b_{\mathbf{k}}^{\dagger}b_{\mathbf{k}}+E_C(k)a_{\mathbf{k}}^{\dagger}a_{\mathbf{k}}+\frac{\Omega_R}{2}\left(a_{\mathbf{k}}^{\dagger}b_{\mathbf{k}}+b_{\mathbf{k}}^{\dagger}a_{\mathbf{k}}\right). \tag{1}$$

In this equation $a_{\mathbf{k}}$ and $b_{\mathbf{k}}$ are the annihilation operators for photons and excitons, respectively; $\mathbf{k}$ is the wave vector of excitons and photons in the layer plane. Because of the translational invariance in the cavity plane, photons can only interact with excitons having the same $\mathbf{k}$. The terms $E_C(k)$ and $E_X(k)$ are, respectively, the cavity and exciton dispersions and Ω_R is the Rabi interaction energy between excitons and photons. The normal modes of $H_{\mathbf{k}}$ that diagonalize the Hamiltonian are called cavity polaritons. The annihilation operators $p_{\mathbf{k}}$, $q_{\mathbf{k}}$ for the lower and upper polaritons are given by

$$p_{\mathbf{k}}=X_k b_{\mathbf{k}}-C_k a_{\mathbf{k}} \tag{2}$$

$$q_{\mathbf{k}}=C_k b_{\mathbf{k}}+X_k a_{\mathbf{k}} \tag{3}$$

where X_k and C_k are the Hopfield coefficients [27]

$$X_k=\left(\frac{\delta_k+\sqrt{\delta_k^2+\Omega_R^2}}{2\sqrt{\delta_k^2+\Omega_R^2}}\right)^{1/2} \tag{4}$$

$$C_k=\left(\frac{\Omega_R^2}{2\sqrt{\delta_k^2+\Omega_R^2}\left(\delta_k+\sqrt{\delta_k^2+\Omega_R^2}\right)}\right)^{1/2} \tag{5}$$

with $\delta_k=E_C(k)-E_X(k)$.

In the presence of strong coupling, when the Rabi frequency Ω_R is larger than the decay rates of the excitons γ_X and of the cavity γ_C, we write the Hamiltonian in the polariton basis

$$H_{\mathbf{k}}=E_{LP}(k)\,p_{\mathbf{k}}^{\dagger}p_{\mathbf{k}}+E_{UP}(k)q_{\mathbf{k}}^{\dagger}q_{\mathbf{k}} \tag{6}$$

where $E_{LP}(k)$ and $E_{UP}(k)$ are the lower and upper polariton dispersions, given by

$$E_{LP(UP)}(k)=\frac{E_C(k)+E_X(k)}{2}-(+)\frac{1}{2}\sqrt{(E_C(k)-E_X(k))^2+\Omega_R^2}\,. \tag{7}$$

The upper and lower branches are separated by an energy gap that is larger than Ω_R.

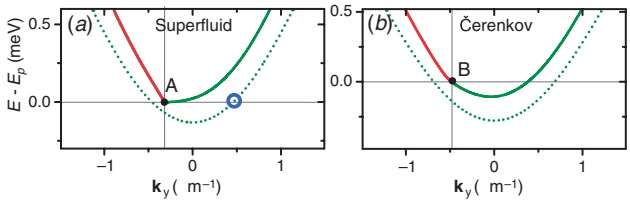

Figure 1. Theoretical polariton dispersion curves. (*a*) Green dotted line: spectrum of excitations under low power non-resonant pumping for $k_p = 0.3\,\mu m^{-1}$ (point A). Injected polaritons can elastically scatter to states with the same energy, as those indicated by the blue circle. E_p is the energy of the pump beam. Solid line: spectrum of excitations under strong pumping for the same k_p. The dispersion curve is blue-shifted due to polariton-polariton interaction. Injected polaritons cannot scatter due to the absence of available final states at the energy of the pump and the system becomes superfluid. The linear part of the curve (in red) is the result of strong modifications due to polariton-polariton interaction. (*b*) Green dotted line: spectrum of excitations under low-power non-resonant pumping for larger pump momentum $k_p = 0.5\,\mu m^{-1}$ (point B). Solid line: spectrum at high density for the same k_p. The linear spectrum of excitations results in a sound velocity smaller than the velocity of the fluid and the Cerenkov regime is reached. (The color version of this figure is included in the online version of the journal.)

We will mainly be interested in the lower polariton. In the low k range, the dispersion shape of the lower polariton is parabolic, as shown in Figure 1(*a*). A nearly resonant laser with a well-defined energy and momentum (point A in Figure 1(*a*)) will mainly excite polaritons in a single point of this dispersion curve. Polaritons injected in this way can scatter elastically to states with the same energy, as the one indicated by the blue circle.

The Coulomb and exchange interactions between the carriers gives rise to exciton-exciton interaction with a Hamiltonian that can be written as [5,28],

$$H_{exc-exc} = \frac{1}{2}\sum_{\mathbf{k},\mathbf{k}',\mathbf{q}} V_q b^\dagger_{\mathbf{k}+\mathbf{q}} b^\dagger_{\mathbf{k}'-\mathbf{q}} b_{\mathbf{k}} b_{\mathbf{k}'} \tag{8}$$

where V_q can be expressed as a function of the quantum well parameters. As long as the nonlinear terms are small compared with the Rabi splitting Ω_R, it is possible to neglect the nonlinear interaction between the upper and lower branches, which yields non-secular terms. The two polariton branches are then virtually decoupled and it is more appropriate to use the polariton basis. In addition, we consider a close to resonance excitation of the lower branch by a monochromatic laser field and we will focus our attention on the evolution of the lower branch polariton. In terms of the lower polariton operators, the Hamiltonian is now $H = H_{LP} + H_{PP}$. The free polariton term is $H_{LP} = \sum_{\mathbf{k}} E_{LP}(k)\, p^\dagger_{\mathbf{k}} p_{\mathbf{k}}$. The effective polariton-polariton interaction term is

$$H_{PP} = \frac{1}{2}\sum_{\mathbf{k},\mathbf{k}',\mathbf{q}} V^P_{\mathbf{q}} p^\dagger_{\mathbf{k}+\mathbf{q}} p^\dagger_{\mathbf{k}'-\mathbf{q}} p_{\mathbf{k}} p_{\mathbf{k}'} \tag{9}$$

where V^P_q is the projection of V_q on the polariton basis. This Hamiltonian gives rise to various types of non-linear optical effects and to parametric generation. Here we will concentrate on the effect of this interaction on the polariton dispersion curve. When the laser intensity is increased, polariton-polariton interactions increase, resulting in the polariton dispersion curves being shifted towards higher energies. This blue shift is due to the repulsive interactions. Moreover, the dispersion curve also becomes strongly distorted as a consequence of collective Bogoliubov-like many-body interactions [20,21]. The evolution of the polariton wavefunction $\psi(x, t)$ is given by the Gross–Pitaevskii equation

$$i\hbar\frac{\partial\psi(\mathbf{x},t)}{\partial t} = \left[E_{LP} - \frac{i\gamma}{2} + V_{\text{def}}(\mathbf{x}) + g|\psi(\mathbf{x},t)|^2\right]\psi(\mathbf{x},t) + F_p e^{i(\mathbf{k_p}\mathbf{x}-\omega_p t)} e^{(\mathbf{x}-\mathbf{x_0})^2/2\delta_x^2} \tag{10}$$

where E_{LP} is the energy of the lower polariton, γ is the decay rate of the polaritons, $V_{\text{def}}(x)$ is the potential that accounts for the defects present in the sample, g is the polariton-polariton coupling strength proportional to V^P_q; F_p is the pumping term, proportional to the amplitude of the pump laser field, with wave vector $\mathbf{k_p}$ and frequency ω_p; x_0 is the position of the center of the Gaussian spot on the sample, with a diameter δ_x.

In a simplified picture, for a specific density $|\psi_c|^2$, from parabolic, the dispersion is predicted to become linear in some k vector range with a discontinuity of its slope in the vicinity of the pump wave-vector k_p, as shown in Figure 1(*a*). Under these conditions, a sound velocity can be attributed to the polariton fluid, given by:

$$c_s = \sqrt{\hbar g|\psi_c|^2/m}\,. \tag{11}$$

If the flow velocity v_p of the polariton fluid, given by $v_p = \hbar k_p/m$ and the frequency of the excitation field are chosen such that the density giving rise to a linearized spectrum of excitations results in $c_s > v_p$, then the Landau criterion for superfluidity is satisfied, as shown in [21]. In such a case, since no states are any longer available for scattering at the frequency of the driving polariton field, as can be seen in Figure 1(*a*), the polariton scattering from the defect is inhibited and the fluid is able to flow unperturbed.

When a polariton fluid with a higher momentum is created using a laser beam with a larger incidence angle, as in Figure 1(*b*), one can enter a different regime.

The Bogoliubov dispersion of collective excitations has a sound-like nature with a sound speed that is now lower than the flow speed ($c_s < v_p$). For the density at which a sound velocity is well defined, the spectrum presents a linearized dispersion together with available states at the same energy and at lower energies than the pump. The defect is able to generate collective Bogoliubov excitations in the fluid. In this case, a Cerenkov-like density modulation pattern is predicted. In the next section we show the experimental demonstration of these effects.

3. Experiment

3.1. Experimental set-up

Our experiment relies on a microcavity sample, cooled at 5 K in which a polariton fluid is excited with a circularly polarized beam from a frequency stabilized, single-mode continuous wave titanium:sapphire laser. The set-up is schematized in Figure 2(*a*). The sample used in this experiment is a GaAs microcavity with a thickness of 2λ, and containing three 8 nm InGaAs quantum wells placed at the maxima of the electromagnetic field of the cavity mode. The two Bragg mirrors forming the cavity are made of alternated λ/4 layers of AlAs and GaAs, with reflectivities between 99.85% and 99.95%. The two mirrors form a wedge (engineered during the microcavity growth), so that the detuning between the cavity and the exciton frequencies can be varied by moving the laser spot on the sample. The wedge angle is about 10^{-6} rad, small enough not to have any effect over the size of the laser spot. The cavity substrate is polished and allows for transmission measurements. In the strong coupling regime, the Rabi splitting is 5.1 meV. The high finesse of this microcavity (≃3000) leads to polariton linewidths of ∼100 μeV at low power excitation.

The laser beam that generates the polaritons is focused onto the sample in a spot of about 100 μm in diameter. Two angles of incidence will be studied : 2.6° and 4.0° (Figure 2(*b*)). The wavelength of the pump laser is close to resonance with the lower polariton branch (≃836 nm). We choose the excitation point on the sample so that the cavity-exciton detuning $\omega_{exc} - \omega_{cav} = -1.1$ meV. The image of the surface of the sample (near-field emission) and of the far field in transmission are simultaneously recorded on two different high resolution CCD cameras. At low power non-resonant excitation, the parabolic dispersion curve characteristic of the lower polariton branch can be observed using an imaging spectrometer, as shown in Figure 2(*b*).

Three key-parameters of the polariton ensemble, the oscillation frequency of the polariton field, the polariton flow velocity, and the polariton density

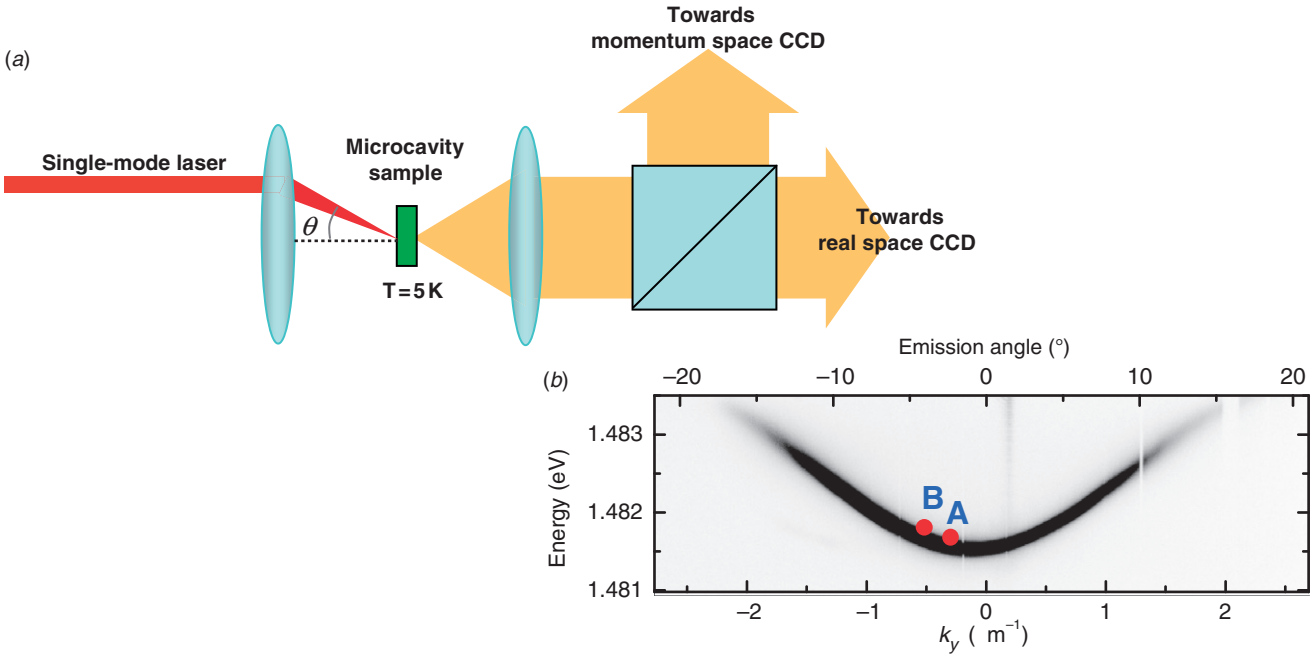

Figure 2. (*a*) Scheme of the experimental excitation and detection conditions. (*b*) Lower polariton branch dispersion, in the regime where interactions are negligible, as observed after non-resonant excitation. Points A and B correspond to the two values of the excitation energy and momentum used in the experiments, $k_p = 0.34\,\mu m^{-1}$ and $0.52\,\mu m^{-1}$. (The color version of this figure is included in the online version of the journal.)

can be fully controlled by adjusting the laser parameters. The polaritons are created with a well-defined energy $\hbar\omega_p$, which is that of the excitation laser. The polaritons have a well-defined momentum $\hbar k_p$, given by the angle of incidence of the laser beam θ_p, through $k_p = \omega_p/c \sin\theta_p$, where c is the speed of light. The quantum fluid properties of the system critically depend on the quantity $g|\psi|^2$, where the particle density $|\psi|^2$ can be changed in a precise way by changing the incident laser power. In this respect, polaritons constitute an ideal system from the experimental point of view, which allows us to finely tune the parameters of the polariton fluid to observe the various regimes predicted by the model.

3.2. *Observation of superfluidity*

In order to study the propagation properties of the injected polariton fluid, the center of the excitation spot is placed on a small defect present in the sample. Such defects appear in the growth process of microcavity samples and we use these defects to study the scattering properties of the polariton flow. We first investigate the situation for a small pump angle of incidence equal to 2.6°, corresponding to a low in-plane momentum of $k_p = 0.34\,\mu m^{-1}$. At low excitation power ($P_I = 5\,mW$) and quasi resonant excitation of the lower polariton branch, polariton-polariton interactions are negligible and polaritons can be considered as independent from each other. In the presence of a 4 μm size defect the coherent polariton gas created by the laser is scattered by the defect and generates a series of cylindrical waves propagating away from the defect (Figure 3(*a*-I)). In the near-field (real space) images, parabolic-like wavefronts around the defect are observed, resulting from the interference of the incident polariton plane-wave with the scattered cylindrical waves. In momentum space, polariton scattering gives rise to the well known Rayleigh ring that is observed in the far-field images (Figure 4(*a*-I)).

As the laser intensity is increased, polariton-polariton interactions increase, resulting in a dramatic change in the polariton flow. The situation is shown in Figure 3(*a*-II) and 3(*a*-III) for the real space images of the polariton fluid. The parabolic interference wavefront disappears, corresponding to the disappearance of the waves scattered by the defect, as predicted by the model. This superfluid regime is first reached in the center of the Gaussian excitation spot for the excitation density corresponding to Figure 3(*a*-II). As the intensity of the excitation laser is increased further, the superfluid condition extends to the rest of the spot

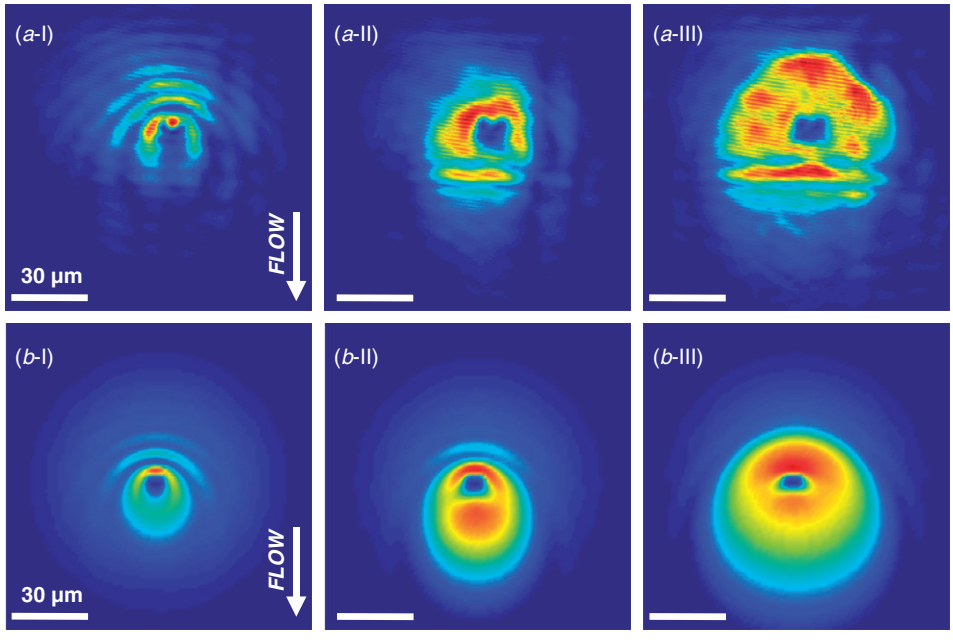

Figure 3. Observation of polariton fluids created with a low in-plane momentum of $0.34\,\mu m^{-1}$ (excitation angle of 2.6°), and an excitation laser blue-detuned by 0.10 meV with respect to the low density polariton dispersion (point A in Figure 2(*b*)). Panel (*a*) depicts the experimental near field images of the excitation spot around a defect for increasing excitation densities. At low pump power P (*a*-I, P_I) the polariton fluid scatters on the defect giving rise to parabolic wavefronts. At higher power the emission pattern is significantly affected by polariton-polariton interactions (*a*-II, $P_{II} = 4P_I$) and eventually shows the onset of a superfluid regime (*a*-III, $P_{III} = 20P_I$). Panel (*b*) shows the corresponding calculated images. (The color version of this figure is included in the online version of the journal.)

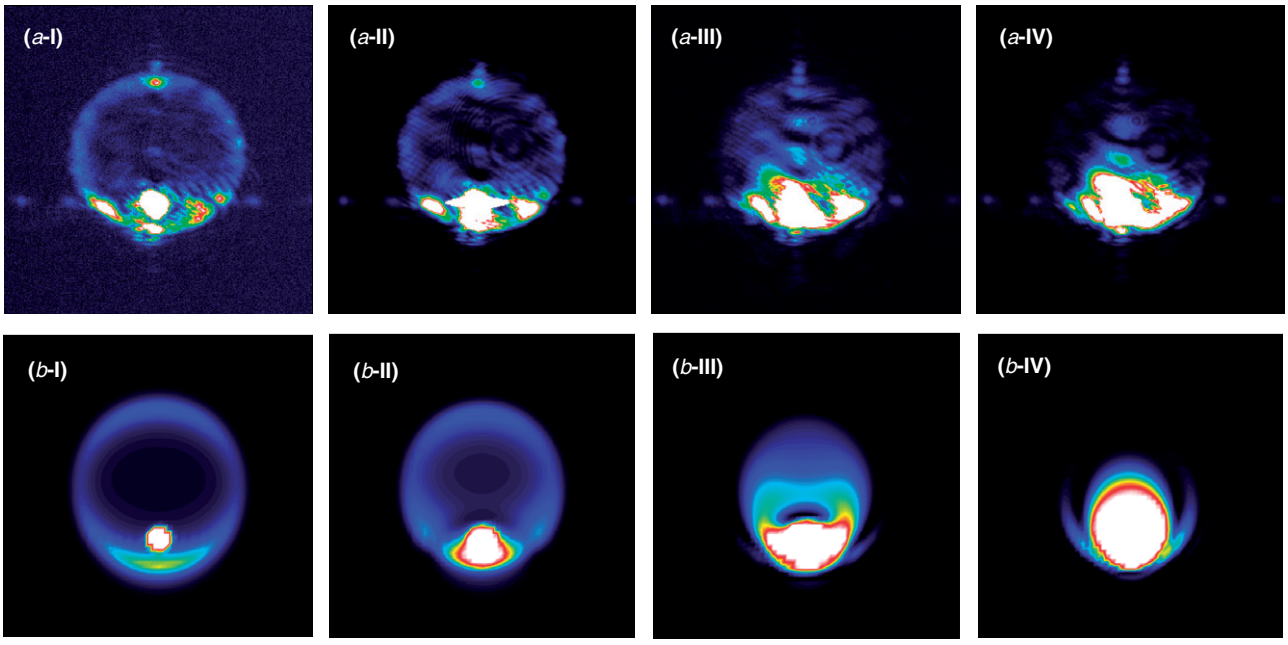

Figure 4. Observation of polariton fluids created in similar excitation conditions as Figure 3. Panels (*a*-I)–(*a*-IV) depict the experimental far field, i.e. momentum space images of the excitation spot around a defect. At low power (*a*-I) the polariton fluid scatters on the defect giving rise to the usual Rayleigh elastic scattering ring. At high powers the approach and eventual onset of a superfluid regime is evidenced by the shrinkage (*a*-II) and collapse (*a*-III, *a*-IV) of the scattering ring. Panel (*b*) shows the corresponding calculated images. (The color version of this figure is included in the online version of the journal.)

(Figure 3(*a*-III)). The non-uniformity in the excitation spot creates a gradient in the polariton concentration that could induce a flow towards the outside of the spot, as in polariton condensates. However, in our case, the main flow direction is induced by the velocity imprinted by the laser excitation, and no effect of an additional flow is observed.

Simulations [21] based on the solution of polariton non-equilibrium Gross–Pitaevskii equation (10) are shown in Figures 3(*b*-I) to 3(*b*-III). The calculations have been performed by adjusting the values of g and $|\psi|^2$ around the experimentally estimated values and by fitting the size and depth of the defect. An optical defect with a depth of 1 meV was assumed in the model, and was found to correspond to experimental observations. The polariton density $|\psi|^2$ is obtained from the experimental emitted intensity and g is estimated from the aperture of the Cerenkov fringes as discussed below. In these figures, one can see a very good agreement between the observed effects and the theory.

The dispersion curve in the presence of a strong laser illumination cannot be recorded because the stray light from the laser prevents the detection of the polariton photoluminescence with the spectrometer. However, a detailed study of the far field emission allows us to check that the observed effect is not a mere suppression of the scattering due to the renormalization of the dispersion curve by the blue shift. In Figure 4 we show the scattered light recorded in the far field for increasing intensities of the pump laser in the upper panel and the corresponding simulations obtained from the model in the lower panel. It can be seen that at low intensities, the laser spot lies slightly inside the Rayleigh ring, since the laser energy is above the dispersion curve (Figure 4(*a*-I)). When the intensity is increased, the dispersion curve undergoes a blue shift towards higher energies, and the laser spot now lies on the ring, which has shrunk slightly (Figure 4(*a*-II)).

When the laser intensity is further increased, the behavior is different. The scattering ring observed at low density collapses (Figure 4(*a*-III) and 4(*a*-IV)) confirming that scattering of the polariton fluid by the defect is inhibited. The laser spot stays on the ring while it collapses, indicating a major deformation in the shape of the dispersion curve. This disappearance of the scattering ring occurs at the same intensity as the one for which the parabolic fringes disappear, and can be attributed to the onset of the superfluid regime. The simulation obtained with the model and shown in the lower panel, Figure 4(*b*-I) to (*b*-IV) are in very good agreement with the observed patterns. In the next section, the observation of Cerenkov waves and the measure of the speed of sound further confirm the behavior of the quantum fluid.

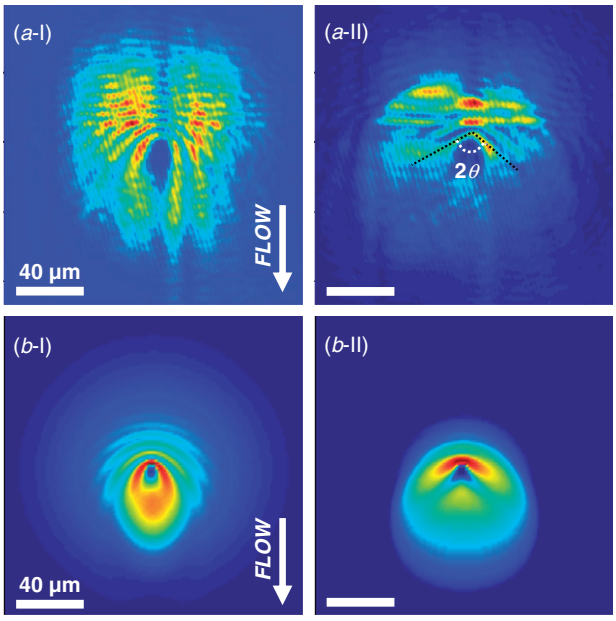

Figure 5. Cerenkov regime. Observation of a polariton fluid created with $k_p = 0.52\,\mu m^{-1}$ (angle of incidence of 4.0°) and an excitation laser blue-detuned by 0.11 meV with respect to the low density polariton dispersion corresponding to point B in Figure 2(*b*). Panel (*a*) shows the experimental near-field images of the excitation spot around a defect, for increasing excitation densities. At low power the emission is characterized by parabolic wavefronts around the defect in real space (*a*-I). As the excitation density is increased (by a factor of 10), the onset of polariton-polariton interactions leads the system to the Cerenkov regime ($c_s < v_p$) characterized by linear wavefronts in real space around the defect (*a*-II). Panel (*b*) shows the corresponding calculated images. (The color version of this figure is included in the online version of the journal.)

3.3. Supersonic regime

In this section, we study the behavior of polaritons created with a higher momentum, which is expected to exhibit a supersonic regime predicted in Section 2. A polariton fluid with a higher momentum is created using a laser beam with a larger incidence angle, of 4.0°, which corresponds to a wave number of $0.52\,\mu m^{-1}$, shown in point B in Figure 2(*b*), and to a flow speed that is larger than the sound speed ($v_p > c_s$).

At low pump power (Figure 5(*a*-I)), the Bogoliubov excitations are similar to single-particle ones, and the parabolic-shaped modulation is observed, as in Figure 3(*a*-I). When the laser intensity and thus the polariton density is increased, the polariton waves are still scattered by the defect (Figure 5(*a*-II)), and one observes interference wave fronts between the incoming and scattered polariton waves. As explained above (Figure 1(*b*)), the calculated spectrum of excitations at high density presents a linearized dispersion, corresponding to a well-defined sound velocity, together with available states at the same and lower energies than the pump. In this case, the defect is able to generate collective Bogoliubov excitations in the fluid. The excitations generate a Cerenkov-like density modulation pattern with characteristic straight wavefronts in the real space images (Figure 5(*a*-II)). A similar density pattern was observed in atomic BECs propagating against the optical potential of a localized defect at supersonic velocities [29]. The calculated images also reproduce these observations as shown in Figure 5(*b*-I) and 5(*b*-II).

The observation of the linear Cerenkov-like wavefronts in Figure 5(*a*-II) is a direct indication of the existence of a well-defined sound speed in the system. The angle of aperture 2θ of the wake profile enables the precise measurement of the sound speed in the system, given by $\sin\theta = c_s/v_p$. In the conditions of Figure 5(*a*-II) we find $c_s = 8.1 \times 10^5\,ms^{-1}$. With the use of Equation (11) the polariton-polariton coupling constant $\hbar g$ can be estimated, being of the order of $0.01\,meV\,\mu m^2$, which is consistent with previously predicted values on the exciton-exciton interaction [30].

4. Conclusion

We have presented a comprehensive set of experiments in different excitation configurations showing evidence for polariton superfluidity in the sense of flow without scattering when traversing an obstacle. Our results under CW resonant excitation can be well described by the Landau model of superfluidity, with the existence of a critical flow velocity for the onset of perturbations in the fluid. Our observations pave the way towards the investigation of a rich variety of quantum fluid effects associated with the non-equilibrium nature of the microcavity polariton system [31].

For example, the fine control of the size and initial state of the polariton condensates through the resonant optical excitation, enables us to address other questions, such as the formation of Josephson oscillations [32] or the formation of quantized vortices in these out-of-equilibrium systems.

Acknowledgements

This work was supported by the Ile de France program IFRAF. A.A. and S.P. were funded by the Agence Nationale pour la Recherche, A.B. is a member of the Institut Universitaire de France.

References

[1] Baumberg, J.J.; Vina, L. Special issue on Semiconductor Microcavities. *Semicond. Sci. Technol.* **2003,** *18,* S279–S434.

[2] Weisbuch, C.; Nishioka, M.; Ishikawa, A.; Arakawa, Y. *Phys. Rev. Lett.* **1992,** *69,* 3314–3317.

[3] Kavokin, A.V.; Malpuech, G. *Cavity Polaritons*; Elsevier: New York, 2003.

[4] Houdré, R.; Weisbuch, C.; Stanley, R.P.; Oesterle, U.; Pellandini, P.; Ilegems, M. *Phys. Rev. Lett.* **1994,** *73,* 2043–2046.

[5] Ciuti, C.; Schwendimann, P.; Deveaud, B.; Quattropani, A. *Phys. Rev. B* **2000,** *62,* R4825–R4828.

[6] Baumberg, J.J.; Savvidis, P.G.; Stevenson, R.M.; Tartakovskii, A.I.; Skolnick, M.S.; Whittaker, D.M.; Roberts, J.S. *Phys. Rev. B* **2000,** *62,* R16247–R16250.

[7] Savvidis, P.G.; Baumberg, J.J.; Stevenson, R.M.; Skolnick, M.S.; Whittaker, D.M.; Roberts, J.S. *Phys. Rev. Lett.* **2000,** *84,* 1547.

[8] Messin, G.; Karr, J.-Ph.; Baas, A.; Khitrova, G.; Houdré, R.; Stanley, R.P.; Oesterle, U.; Giacobino, E. *Phys. Rev. Lett.* **2001,** *87,* 127403.

[9] Baas, A.; Karr, J.-Ph.; Romanelli, M.; Bramati, A.; Giacobino, E. *Phys. Rev. B* **2004,** *70,* 161307(R).

[10] Karr, J.P.; Baas, A.; Houdré, R.; Giacobino, E. *Phys. Rev. A* **2004,** *69,* 031802(R).

[11] Karr, J.-Ph.; Baas, A.; Giacobino, E. *Phys. Rev. A* **2004,** *69,* 063807; Romanelli, M.; Karr, J.-Ph.; Leyder, C.; Giacobino, E.; Bramati, A. Phys. Rev. Lett. **2007,** 98, 106401.

[12] Leyder, C.; Liew, T.C.H.; Kavokin, A.V.; Shelykh, I.A.; Romanelli, M.; Karr, J.Ph.; Giacobino, E.; Bramati, A. *Phys. Rev. Lett.* **2007,** *99,* 196402.

[13] Moskalenko, S.A.; Snoke, D.W. *Bose–Einstein Condensation of Excitons and Biexcitons and Coherent Nonlinear Optics with Excitons*; Cambridge University Press: Cambridge, 2000.

[14] Malpuech, G.; Rubo, Y.G.; Laussy, F.P.; Bigenwald, P.; Kavokin, A.V. *Semicond Sci. Technol.* **2003,** *18,* S395.

[15] Keeling, J.; Eastham, P.R.; Szymanska, M.H.; Littlewood, P.B. *Phys. Rev. Lett.* **2004,** *93,* 226403.

[16] Kasprzak, J.; Richard, M.; Kundermann, S.; Baas, A.; Jeambrun, P.; Keeling, J.M.J.; Marchetti, F.M.; Szymanska, M.H.; André, R.; Staehli, J.L.; Savona, V.; Littlewood, P.B.; Deveaud, B.; Dang, L.S. *Nature* **2006,** *443,* 409–414.

[17] Balili, R.; Hartwell, V.; Snoke, D.; Pfeiffer, L.; West, K. *Science* **2007,** *316,* 1007–1010.

[18] Lagoudakis, K.G.; Wouters, M.; Richard, M.; Baas, A.; Carusotto, I.; André, R.; Dang, L.S.; Deveaud-Plédran, B. *Nature Phys.* **2008,** *4,* 706–710.

[19] Sanvitto, D.; Marchetti, F.M.; Szymańska, M.H.; Tosi, G.; Baudisch, M.; Laussy, F.P.; Krizhanovskii, D.N.; Skolnick, M.S.; Marrucci, L.; Lemaître, A.; Bloch, J.; Tejedor, C.; Viña, L. *Nature Phys.* **2010,** *6,* 527–533.

[20] Carusotto, I.; Ciuti, C. *Phys. Rev. Lett.* **2004,** *93,* 166401.

[21] Ciuti, C.; Carusotto, I. *Phys. Stat. Sol. (b)* **2005,** *242,* 2224–2245.

[22] Amo, A.; Lefrère, J.; Pigeon, S.; Adrados, C.; Ciuti, C.; Carusotto, I.; Houdré, R.; Giacobino, E.; Bramati, A. *Nature Phys.* **2009,** *5,* 805–810.

[23] Amo, A.; Sanvitto, D.; Laussy, F.P.; Ballarini, D.; Valle, E.D.; Martin, M.D.; Lemaître, A.; Bloch, J.; Krizhanovskii, D.N.; Skolnick, M.S.; Tejedor, C.; Viña, L. *Nature* **2009,** *457,* 291–295.

[24] Leggett, A.J. *Rev. Mod. Phys.* **1999,** *71,* S318–S323.

[25] Onofrio, R.; Raman, C.; Vogels, J.M.; Abo-Shaeer, J.R.; Chikkatur, A.P.; Ketterle, W. *Phys. Rev. Lett.* **2000,** *85,* 2228–2231.

[26] Raman, C.; Köhl, M.; Onofrio, R.; Durfee, D.S.; Kuklewicz, C.E.; Hadzibabic, Z.; Ketterle, W. *Phys. Rev. Lett.* **1999,** *83,* 2502–2505.

[27] Hopfield, J. *Phys. Rev.* **1958,** *112,* 1555–1567.

[28] Ciuti, C.; Schwendimann, P.; Quattropani, A. *Phys. Rev. B* **2001,** *63,* 041303(R).

[29] Carusotto, I.; Hu, S.X.; Collins, L.A.; Smerzi, A. *Phys. Rev. Lett.* **2007,** *97,* 260403.

[30] Ciuti, C.; Savona, V.; Piermarocchi, C.; Quattropani, A.; Schwendimann, P. *Phys. Rev. B* **1998,** *58,* 7926–7933.

[31] Wouters, M.; Carusotto, I. *Phys. Rev. Lett.* **2010,** *105,* 020602.

[32] Sarchi, D.; Carusotto, I.; Wouters, M.; Savona, V. *Phys. Rev. B* **2008,** *77,* 125324.